EFFECT OF GRAPHENE COATINGS AND WATER TEMPERATURE ON MARINE BIOFOULING SYSTEMS

by

Ke Jia

Submitted in partial fulfilment of the requirements
for the degree of Master of Applied Science

at

Dalhousie University
Halifax, Nova Scotia
August 2022

TABLE OF CONTENTS

LIST OF TABLES

LIST OF FIGURES

ABSTRACT

This work investigated two strategies for controlling marine biofouling. One method involved the use of graphene-enhanced coatings to mitigate biofilm growth. The second study assessed the influence of water temperature on biofouling. Biological annular reactors (ARs) were used to imitate the marine environment and microbiological tests, such as adenosine triphosphate (ATP), heterotrophic plate counts (HPC), protein and carbohydrate concentrations in extracellular polymeric substance (EPS) were used to assess the biofilm accumulation. Graphene-enhanced coatings demonstrated the potential to reduce biomass accumulation. In addition, though higher water temperature accelerates bacterial growth, the bacterial growth efficiency would decline, which leads to less biomass.

LIST OF ABBREVIATIONS AND SYMBOLS USED

AR	Annular reactor
ATP	Adenosine triphosphate
BSA	Bovine serum albumin
BSC	Biological safety cabinet
cATP	Cellular adenosine triphosphate
CFU	Colony forming units
DSA	Deposit & surface analysis
EDTA	Ethylenediaminetetraacetic acid
EPS	Extracellular polymeric substances
FR	Fouling release
GC111	GrapheneCoat111
GC112	GrapheneCoat112
GIT	Graphite Innovation and Technologies
HDPE	High-density polyethylene
HPC	Heterotrophic plate count
HRT	Hydraulic retention time
NTU	Nephelometric turbidity units
PBS	Phosphate buffered saline
QGA	Quench-gone aqueous
Re	Reynolds number
RLU	Relative light unit
RPM	Revolutions per minute
rRNA	Ribosomal ribonucleic acid
tATP	Total adenosine triphosphate
TBT	Tributyltin
Tris	Trisaminomethane

ACKNOWLEDGEMENTS

I would like to thank my supervisor, Dr. Graham Gagnon. I really appreciate the opportunity he has given to me to complete this project and I am very grateful for his g and encouragement during the research period. I would also like to thank my supervisory committee—Dr. Amina Stoddart and Dr. Kevin Plucknett— who provided important comments and feedback.

I also recognize the funding through the NSERC / Halifax Water Industrial Research Chair program and its member partners. I acknowledge the support from Nova Scotia Power Company for this work.

I would like to express my sincere gratitude to Carolina Ontiveros and Sebastian Munoz for teaching me the methods of microbiological experiments. I would also like to thank everyone at the CWRS Group at Dalhousie University for their suggestions, technical support and encouragement.

CHAPTER 1 INTRODUCTION

1.1 BACKGROUND

Biofouling, the accumulation of unwanted marine organisms on submerged surfaces, has negative impacts on many marine industries. Particularly, in the shipping industry, biofouling can cause large energy penalties because of the increased roughness, increased fuel consumption, loss of maneuverability in vessels, etc. (Bressy & Lejars, 2014; Callow & Callow, 2011; Lejars et al., 2012; Chambers et al., 2006). The settlement of marine organisms in piping systems can also cause clogging in heat exchangers, which leads to extra costs in power plants (Rosenhahn, 2010).

Controlling marine biofouling is challenging, mainly due to the vast biodiversity of marine organisms and the large range of adhesion mechanisms (Callow & Callow, 2011). Salinity, water temperature, nutrient concentrations, flow rates, pH, and some other factors of seawater conditions, as well as the surface roughness and substrate material, can affect the formation of biofilm (Bressy & Lejars, 2014; Lejars et al., 2012).

Surface functionalization strategies have been proved to control microbial attachment by adjusting surface roughness, surface hydrophilicity or charge during previous studies (Cheng et al., 2019). Biocidal antifouling paints have been widely used to control biofouling through modifying the material's surface or relying on the release of biocides to hinder the growth of organisms, among which tributyltin (TBT) is the most popular one (Gittens et al., 2013). However, these toxic antifoulants have been banned as they posed heavy environmental risks (Chambers et al., 2006). Therefore, alternative methods have been developed for marine biofouling control. Graphene based materials have been investigated and applied as enhanced anti-fouling coatings as they show superb anti-corrosion, antibacterial and hydrophobic properties (Lu et al., 2017; Nine et al., 2015; Krishnamoorthy et al., 2014).

Water temperature is a critical factor in controlling biofilm formation, as it can change water viscosity, and modify hydrophobicity and surface charge (Farhat et al., 2016; Shao

et al., 2019). Considering the biodiversity of biofouling composition, fouling organisms make different responses in their adhesion properties when the water temperature changes (Pompermayer & Gaylarde, 2000). Consequently, it becomes complex to identify the influences of water temperature on marine biofouling.

1.2 RESEARCH OBJECTIVES

The research outlined in this thesis divided into two sections to identify the influences of graphene coatings and water temperature on marine biofouling.

The first study compared and assessed the antifouling properties of two types of graphene-enhanced coatings by comparing the biofilm formation on the surface of polycarbonate coupons with no coatings and graphene-coated coupons.

The second study assessed the effect of water temperature on biofilm growth by comparing the biofilm formation on the surface of coupons submerged in marine water of different water temperature.

CHAPTER 2 LITERATURE REVIEW

2.1 MARINE BIOFOULING

Marine biofilms are mainly composed of bacteria, diatoms, algae spores and other micro-organisms, which are embedded in a matrix of Extracellular polymeric substances (EPS) (Salta et al., 2013). Microfouling refers to the attachment of biofilm onto wet surfaces, allowing for larger organisms, such as barnacles, mussels, algae to adhere to the wet surface as well, which is referred to as macrofouling (Bressy & Lejars, 2014; Lejars et al., 2012).

Marine biofouling, including both micro- and macro-fouling, refers to the undesired colonization of marine organisms on immersed surfaces in ocean water (Callow & Callow, 2011; Chambers et al., 2006), which follows the same steps (Figure 2.1). Firstly, a conditioning film is formed on the surface with the initial attachment of organic molecules. Subsequently, bacterial organisms adhere to the surface and create a matrix of EPS, which leads to the micro- and macro-organisms attaching to the surface (Chambers et al., 2006 ; Lejars et al., 2012). According to Chambers et al. (2006), the formation of EPS can envelope and anchor the colonizing organisms to the substrate, which changes the surface chemistry, stimulating the further growth of biofilm (Chambers et al., 2006 ; Lejars et al., 2012).

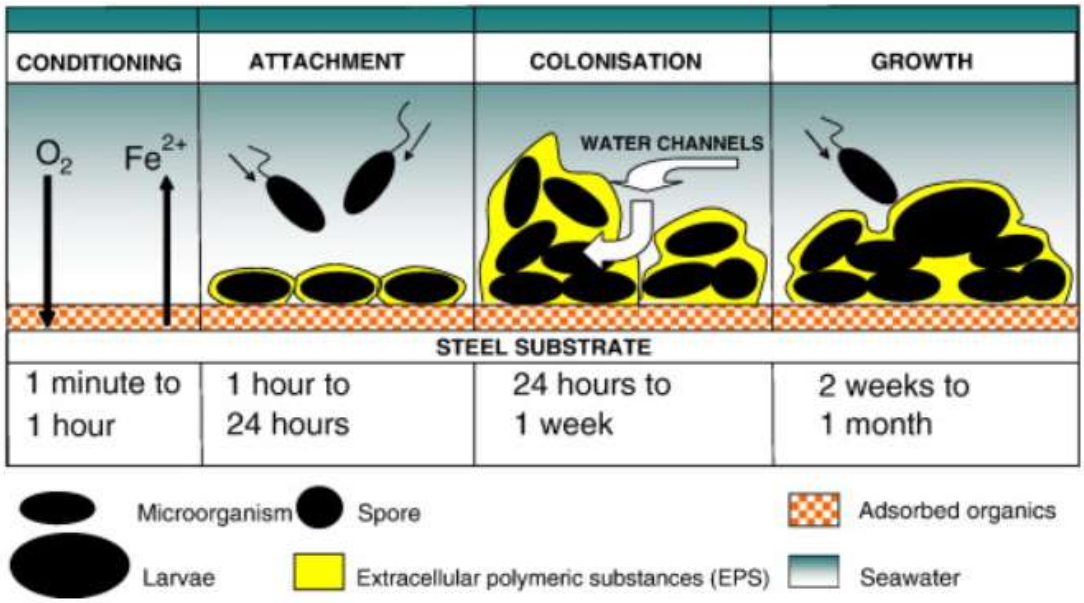

Figure 2.1. Organization of research topics (adapted from Chambers et al.,2006).

Marine biofouling has negative effects on many industries. In the shipping industry, the colonization of marine organisms on submerged surfaces can generate increased surface roughness, increasing the drag resistance between the ship surfaces and water, thus leading to surface deterioration, energy consumption, and the significant increase of fuel consumption and greenhouse gas emissions (Callow & Callow, 2011; Bressy & Lejars, 2014).

2.2 ANTIFOULING CONTROL

2.2.1 Historic Antifouling Techniques

To minimize the fouling on ship hulls, toxic antifoulants were widely used in the past, such as tar, wax, lead, arsenic and other heavy metals and their organic derivatives (Chambers et al., 2006). In the 1960s, self-polishing systems containing tributyl tin (TBT) were developed as effective biocide-releasing paints with moderate price and sustained efficiency. However, the TBT-compounds were subsequently banned, as their toxicity had adverse effects on the marine environment and aquatic life (Lejars et al., 2012; Yang et al., 2014). Therefore, environmentally friendly alternatives have been introduced for antifouling.

2.2.2 Modern Antifouling Methods

There are two main types of antifouling coatings: chemically active coatings and non-toxic fouling release coatings (Bressy & Lejars, 2014). Chemically active antifouling coatings can release biocides, which are tin-free active compounds to act on the marine organisms, thus controlling the settlement of marine organisms (Lejars et al., 2012). Fouling release coatings do not contain any biocides and they can inhibit the bacterial adhesion without chemical reactions. They show great fouling release and non-stick properties, which can reduce the adhesion strength and stimulate the removal of biofilm through hydrodynamical stress during navigation or a simple mechanical cleaning (Bressy & Lejars, 2014; Lejars et al., 2012; Gittens et al., 2013). Graphene-based materials are receiving growing interest in applications for anti-fouling coatings due to the corrosion resistance in seawater, anti-

bacterial and anti-fouling properties (Krishnamoorthy et al., 2014).

2.2.3 Application of Graphene-based Materials in Biofouling Control

Graphene has proven to be widely applicable in different fields during recent years. Graphene is an sp2-hybridized carbon allotrope with tightly packed honeycomb two-dimensional lattice, which demonstrates high surface area and conductivity, chemical inertness, along with remarkable mechanical, physical and chemical properties (Balakrishnan et al., 2020; Manderfeld et al., 2021). The functionalization of graphene, including chemical modification, covalent and noncovalent interactions, has been studied to realize the great application potential (Georgakilas et al., 2012). Graphene oxide (GO), generated via the chemical oxidation of graphite, is a common method to functionalize graphene, which has shown superb antimicrobial properties in several studies (Perreault et al., 2015).

The antimicrobial activity of GO can be ascribed to both physical and chemical interactions, including cell membrane disruption and oxidative stress (Chen et al., 2014). More specifically, the cell membrane can be penetrated by the atomically sharp edges of graphene. Furthermore, the lipid peroxidation due to the oxidative stress of GO can cause membrane damage (Chen et al., 2014; Perreault et al., 2015; Akhavan et al., 2010; Krishnamoorthy et al., 2012). Therefore, graphene-based surfaces are shown to reduce bacterial attachment on the surface.

2.3 EFFECT OF WATER TEMPERATURE ON BIOFOULING

Water temperature has a significant effect on bacterial cell attachment and bacterial growth rate. Water temperature can modify hydrophobicity and microbial cell surface charge, thus affecting initial cell attachment (Van Loosdrecht et al., 1990). According to the experiments conducted by Pompermayer and Gaylarde (2000), some bacteria (e.g., *Staphylococcus aureus*) show better adhesion performance at higher water temperature, while other bacteria (e.g., *Escherichia coli*) adhere better at lower water temperature. Water temperature can also affect the EPS and the EPS matrix viscosity would be decreased under warmer conditions (Lewis et al., 1989; Morimatsu et al., 2012). In addition, water temperature

might further influence changes in bacterial community composition (Lindström et al., 2005).

Higher water temperature has been proved to make a stimulating impact on bacterial growth and metabolism, and to promote the enzymatic activities of bacterial cells for the degradation of organic matter (Brown et al., 2004; Amthor, 1984). Bacterial biofilm biomass might increase at higher water temperature in the exponential bacterial growth phase, while the biofilm growth would be nutrient limited at the end of this phase. Though the biofilm growth rates are expected to increase under higher water temperature, the bacterial growth efficiency might decrease, which leads to less biomass in longer period (Ratkowsky et al., 1982; Sand-Jensen et al., 2007).

CHAPTER 3 MATERIALS AND METHODS

This section will include the materials and methods used to monitor and quantify biofilm growth and the relevant water quality parameters of the growth medium, seawater that were measured.

3.1 ANNULAR REACTOR SYSTEM

3.1.1 Annular Reactor System

Rotating annular reactors (ARs) - from Biosurface Technologies Cord, Bozeman, USA (model 1320LJ) are used to simulate seawater systems to investigate biofilm growth, as the reactors can ensure an uniform distribution of bacteria in the bulk phase, constant distribution of the wall shear stress, well-defined hydrodynamic conditions and flow regimes, etc. (Saur et al., 2017).

The ARs consist of two concentric cylinders: a stationary glass outer cylinder and a rotating inner polycarbonate cylinder. Twenty removable slides are flush mounted on the internal, slotted cylinder which rotates via a variable speed motor (Figure 2.1). The polycarbonate coupons can support biofilm growth, and then be extracted from the reactors and analyzed for microbiological parameters in this research.

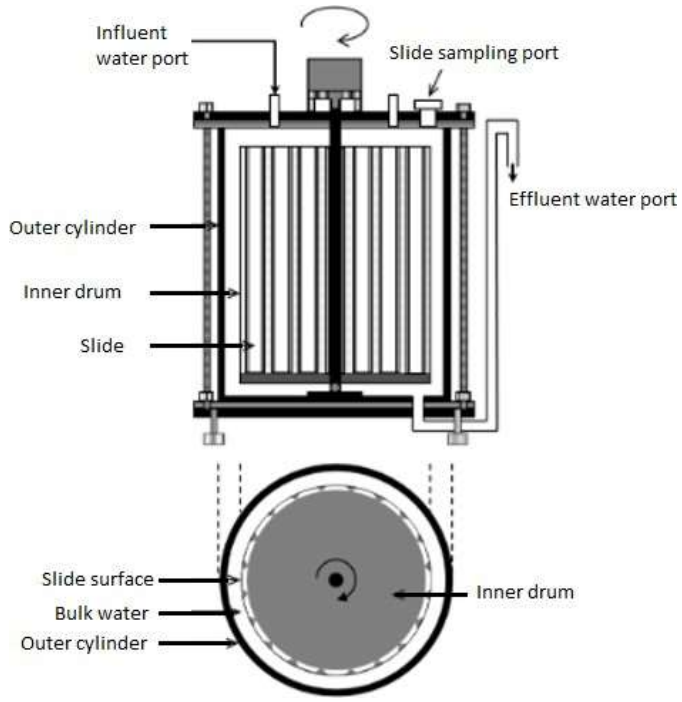

Figure 3.1 Schematic diagram of the AR system (adapted from Park et al., 2015).

Water is pumped via peristaltic pumps (Cole-Parmer Canada Company, QC, Canada) through the influent water port into the area between the inner drum and the outer cylinder of the ARs. The water then flows through the effluent pipeline, which is placed above the effluent water port

to control the hydraulic head. The shear stress (τ) exerted on the surface of the coupons is controlled by the rotational speed of the system, while the hydraulic retention time (HRT) for these reactors is controlled by the volumetric flow rate of the influent water ports.

According to Saur et al. (2017), the following equations can be used to estimate the shear stress (τ) on the surface of the inner cylinder of the ARs:

$$\tau = 2.13 \frac{\left(\frac{r_i}{r_e}\right)^{\frac{3}{2}}}{\left(1-\frac{r_i}{r_e}\right)^{\frac{7}{4}}} Re^{1.445} \frac{\rho v^2}{2\pi {r_i}^2} \qquad \text{for } Re > 800$$

Equation 3.1

$$\tau = 0.113 \frac{\left(\frac{r_i}{r_e}\right)^{\frac{3}{2}}}{\left(1-\frac{r_i}{r_e}\right)^{\frac{7}{4}}} Re^{1.764} \frac{\rho v^2}{2\pi {r_i}^2} \qquad \text{for } Re > 10^4$$

Equation 3.2

where ρ is the density of water (kg/m3), υ is the kinematic viscosity of water (m2/s), ri is the radius of the inner cylinder (m), re is the radius of the outer cylinder (m), and Re is the dimensionless Reynolds number, defined as:

$$Re = \frac{\Omega r_i \delta}{v}$$

Equation 3.3

where Ω is the angular speed of the inner cylinder (rad/s), and δ is the gap between the inner and outer cylinders (m).

3.1.2 Hydrodynamic Conditions

The volume capacity of the annular reactor is about 940 ml.

The retention time of the system was computed using the following equation:

$$\theta = \frac{V}{Q}$$

Equation 3.4

where:

θ = hydraulic retention time (min),

V = volume (mL),

Q = volumetric flow rate (mL/min).

The HRT of the reactors was chosen to be 120 minutes (two hours), which is the maximum recommended retention time according to the operator's manual from BioSurface Technologies Corporation, yielding a flow rate of 7.83 mL/min. This HRT duration has

been commonly used in experiments to assess biofilm growth under different operational conditions and water treatment (Gagnon & Slawson, 1999; Pintar & Slawson, 2003; Park et al., 2015)All the reactors were operated at a rotational speed of 60 rpm to achieve a simulated shear stress of 0.15 N/m^2 (Saur et al., 2017).

3.1.3 Set-up Protocol

Prior to the experiment operation, the reactors, fittings, coupons and tubes were cleaned and sterilized. To achieve this, the components were thoroughly cleaned with antibacterial soap and then rinsed with deionized water. All non-metal components of the ARs were soaked in 10% Nitric Acid for 24 hours and then rinsed with deionized water to ensure the removal of all metal contamination. After cleaning, the assembled reactors and the fittings were autoclaved at 121°C for 15 minutes and placed in the biological safety cabinet (BSC) for cooling. The coupons were inserted into their corresponding slots on the inner cylinder of the ARs, inside of the BSC, and the flow breaks and filters were put in place. In addition, the non-opaque surface was covered with aluminum foil to reduce phototrophic growth within the reactors (Zhu et al., 2014). After proper equipment setup, the reactor systems operated at 60 RPM with deionized water for 2 hours, and then the ocean water was distributed into the ARs at a flow rate of 7.8 mL/min by calibrating the peristaltic pumps (Cole- Parmer Canada Company, QC, Canada). The ARs were allowed to run for 14 days before preliminary sampling to ensure biofilm growth (Zhu et al., 2014).

3.2 SOURCE WATER AND SYSTEM SET-UP

3.2.1 Source Water

100% filtered ocean water was used to feed the ARs and investigate the application of graphene-enhanced coatings and the influence of water temperature to manage marine biofouling. Filtered ocean water from the Halifax Harbor, Nova Scotia, Canada, was collected twice a day in 20-L plastic carboys at the Aquatron Center from Dalhousie University before April 26th, 2021. During April 26th and June 25th, due to the closure of Aquatron Center, the ocean water was collected from Point Pleasant Park and then filtered

through a capsule filter, the filter size of which was the same as that in the Aquatron Center (i.e., 25 μm).

3.2.2 Environmental Set-up

The ARs were connected in parallel to asses the effects of graphene-enhanced coatings and water temperature on biofouling. After operation, the biofilms were extracted from the coupons for microbiological tests. The (proprietary) graphene-enhanced coatings were prepared by Graphite Innovation and Technologies (GIT) company (Halifax, NS, Canada). More detailed description of the experimental set-up is explained in Chapter 4 and Chapter 5.

3.3 WATER SAMPLE COLLECTION AND ANALYSIS

The influent and effluent from each AR was collected in 500-mL high-density polyethylene (HDPE) bottles weekly to test for turbidity, pH and ATP. The HDPE bottles were soaked in 10% (v/v) nitric acid for 24 hours and then rinsed with deionized water before being used.

3.3.1 Analytical Methods

The turbidity of each sample was measured three times using a TL2300 Turbidimeter (HACH Company, Colorado, United States). An Accumet Excel XL50 probe (Fisher Scientific. MA, United States) was used to measure the pH of the samples.

Cellular adenosine triphosphate (cATP) was used to evaluate the microbial activity of the aqueous samples, which was measured using LuminUltra Technologies'(New Brunswick, Canada) Quench-Gone Aqueous (QGA) test kit and protocol, along with their PhotonMaster luminometer. 50-mL sample of the water was obtained by a 60-mL syringe and passed through a filter attached to the bottom of the syringe. 1-mL of UltraLyse 7 was transferred into the syringe after removing the filter. The filter was then re-attached, and

the contents of the syringe were passed through the filter and into a 9-mL dilution tube. Next, 100 µL of the contents in the dilution tube and 100 µL enzyme were transfered into a 12x55 mm test tube. Finally, the test tube was placed in the luminometer and the activity was recorded in Relative light units (RLU). RLU measured were converted to ATP concentrations (pg ATP mL^{-1}) using LuminUltra's conversion formula (the detection limit for this method is 10 RLUs):

$$\mathrm{cATP} = \frac{\mathrm{RLU_{cATP}}}{\mathrm{RLU_{ATP1}}} \cdot \frac{10{,}000}{\mathrm{V_{sample}}}$$

Equation 3.5

where:

cATP = cellular ATP from living biomass (pg ATP/mL),

RLU_{cATP} = microbial activity of Luminase (RLU),

RLU_{ATP1} = microbial activity of sample (RLU),

10,000 = unit conversion factor (pg ATP)

V_{sample} = volume of sample passed through filter (mL).

3.4 BIOFILM COLLECTION AND ANALYSIS

Coupons were removed from each AR after the acclimation period of 14 days(Gagnon & Slawson, 1999).

The outside of the reactors was sprayed and wiped down with 70 % (v/v) ethanol before removing the coupons with a flame sterilized metal hook. Immediately upon removal, the coupons were placed in autoclaved 150 mL capped test tubes, and each test tube was filled with effluent water to prevent the biofilm from drying.

According to Gora et al.(2019), swabbing was shown to be superior to scraping for the removal of biofilm from the coupons. Figure 3.1 below showed the methodology for biofilm recovery and resuspension for total ATP analysis. After removing the coupons, the exposed area of the coupons was divided into three parts to collect biofilm samples. Sterile swabs were then used to swab each section (approximately 5.2 cm^2), as indicated below,

and the swabbing process was repeated five times. The collected biofilms were then submerged into different dilution media: extraction dilution substance for total ATP analysis, phosphate-buffered saline (PBS) solution for heterotrophic plate counts (HPC), and EPS extraction buffer solution for protein and carbohydrates quantification. Next, the samples were vortexed to distribute the biofilm-bound bacteria in the resuspension fluid.

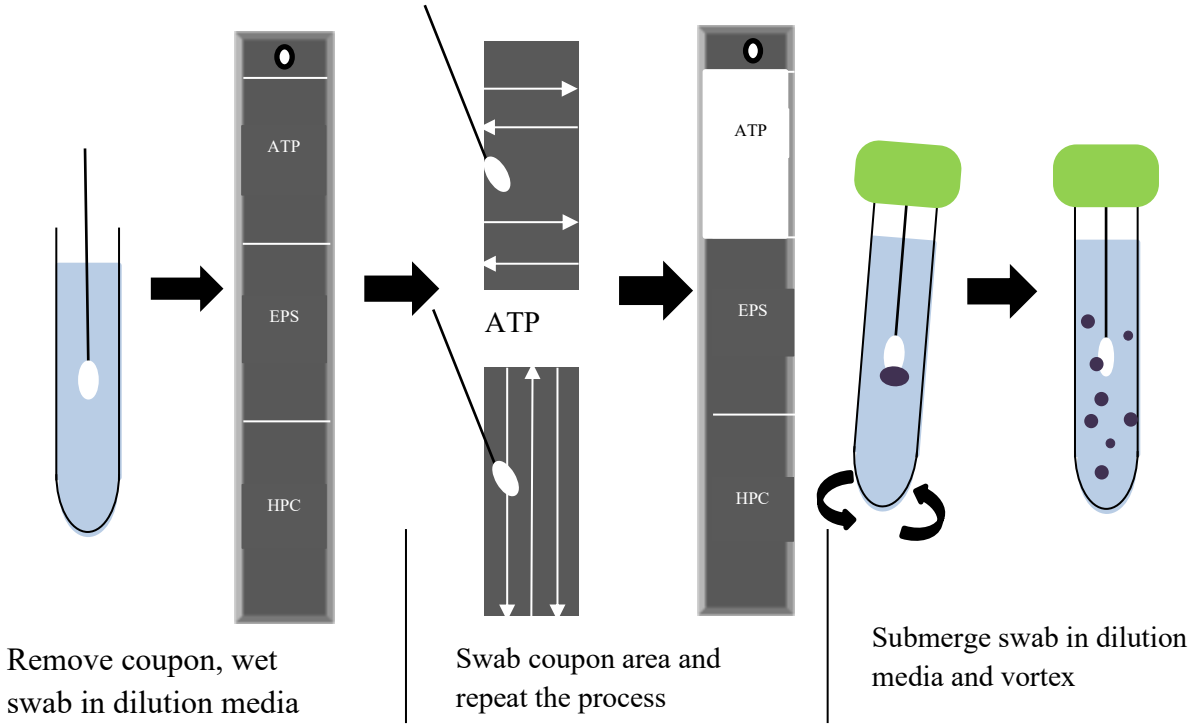

Figure 3.2 Adopted methodology for biofilm recovery, and resuspension (Gora et al., 2019).

After collecting biofilms from the coupons, the coupons were cleaned with phosphorus-free detergent, and then rinsed with deionized water and disinfected with 70% (v/v) ethanol. The uncoated coupons were also autoclaved at 121°C for 15 minutes, while the graphene-coated coupons were not autoclaved in case of the degradation of the coating material. Finally, the coupons were re-inserted into their corresponding ARs.

All microbiological tests were performed in the BSC to limit biological contamination of samples and maintain sterility of materials.

3.4.1 Adenosine Triphosphate Analysis

Total adenosine triphosphate (tATP), an indicator of microbiological activity, was measured using LuminUltra's Deposit and Surface Analysis (DSA) test kit for the swabbed biofilm. As shown in Figure 3.1, tATP was measured by extracting the biofilm from one third of the exposed surface area of the coupons (5.2 cm^2). The collected biofilms were analysed with the PhotonMaster luminometer to obtain tATP concentrations. The results obtained from the luminometer were converted by using LuminUltra's conversion formula (the detection limit for this method is 10 RLUs):

$$\mathrm{tATP} = \frac{\mathrm{RLU_{tATP}}}{\mathrm{RLU_{ATP1}}} \cdot \frac{50{,}000}{\mathrm{A_{collector}}}$$

Equation 3.6

where:

tATP = total ATP from living and non-living biomass (pg ATP/cm^2),

RLU_{tATP} = microbial activity of Luminase (RLU),

RLU_{ATP1} = microbial activity of sample (RLU),

50,000 = unit conversion factor (pg ATP)

$A_{collector}$ = surface area of the biofilm-containing area (cm^2).

3.4.2 Heterotrophic Plate Counts

The heterotrophic plate count (HPC) method is used to quantify the culturable microbes from the biofilm accumulated on the coupons. The removed biofilm from one third of the exposed surface area of the coupons (5.2 cm^2) was submerged into a 5 mL sterile PBS solution and then vortexed for 30 seconds to distribute the biofilm-bound bacteria in the resuspension fluid. The PBS solution was prepared following the *Standard Method* 9050C1a (APHA, AWWA & WEF 2012) and then autoclaved at 121°C for 15-min.

According to Standard Methods 9215C (AHPA, 2012), ten-fold serial dilutions were spread-plated, in triplicate, using 0.1 to 1 mL diluted sample. The culture media was

composed of Zobell marine agar 2216 (HiMedia Laboratories, India), which was prepared in deionized water, following manufacturer's instructions, and then autoclaved at 121 °C for 15 min. A volume of 100 µL was pipetted onto the solid gelled agar and spread by means of an ethanol flame sterilized glass rod. The agar plates were then incubated in the dark for 7 days at room temperature (19 ± 2 °C). Finally, the number of colonies that grew on each plate was recorded. According to the American Public Health Association (APHA) Method 9215 (2004), only plates having 30 to 300 colonies should be considered, while others should be disregarded.

To account for the dilution factor of the plate and the volume of biofilm solution that was pippeted onto the agar plate, the following equation is used:

$$\text{HPC1} = \frac{\text{Colonies Counted}}{\text{Volume plated}} \cdot \text{Dilution Factor}$$

Equation 3.7

where:

HPC1 = heterotrophic plate count (CFU/mL),

Volume plated = actual volume of sample plated (mL),

Dilution Factor = dilution of sample plated.

Finally, biofilm HPCs were reported as CFU cm^{-2} by using the following equation:

$$\text{HPC} = \frac{\text{HPC1}}{\text{Sample Area}} \cdot \text{Total Volume}$$

Equation 3.8

where:

HPC = heterotrophic plate count (CFU/cm^2),

Sample Area = coupon area swabbed (cm^2),

Total Volume = total volume of PBS used to collect biofilm (mL).

3.4.3 Extracellular Polymeric Substances

Extra Polymeric Substances are the primary constituent of biofilm, which is primarily composed of carbohydrates and proteins. The extracellular matrix is a complex and extremely important component of all biofilms, as it provides architectural structure and mechanical stability to the attached biomass (Allison, 2003;Flemming & Wingender, 2010).

Similarly, one third of the total area of the coupons was swabbed and then resuspended in 10 mL of an EPS extraction buffer solution (10 mM Tris, 10 mM EDTA, 2.5% NaCl, pH 8). The collected biofilms in the EPS solution were vortexed for 1 min and then incubated in a shaking incubator for 4 hours at 35℃ and 200 rpm. The falcon tubes were then centrifuged at 3600 g for 10 minutes and, in each case, the supernatant was filtered using 0.45 µm cellulose nitrate filters to collect the EPS component in the filtrate. The samples were placed in a freezer (below -20 ℃) and analyzed once all samples were collected.

For carbohydrate quantification, glucose was used as the standard. Several dilutions of glucose in water were prepared, as well as mixtures of 150 µL of the sample, 450 µL H_2SO_4 and 90 µL of 5% phenol. The solutions were incubated for 10 minutes at 90°C, and then 200 µL of each solution was transferred to a 96 well plate in duplicate to measure the absorbance at 490 nm by the microplate reader. For protein quantification, bovine serum albumin (BSA) was used as the standard. A mixture of 50 µL of the sample and 400 µL of the working reagent was vortexed and then incubated at 60°C for 30 minutes. 200 µL of each dilution was transferred to a 96 well plate in duplicate to measure the absorbance at 562 nm by the microplate reader. The absorbance values were then converted to concentration values according to the standard curves obtained. To convert the concentrations into more appropriate units that take into account the size of the coupons, the following equation was used:

$$\mathrm{C} = \frac{C_1}{\text{Sample Area}} \cdot \text{Total Volume}$$

Equation 3.9

where:

C = concentration (µg/cm^2),

C_1 = concentration (µg/L)

Sample Area = coupon area swabbed (cm^2),

Total Volume = total volume of buffer used to collect biofilm (L).

CHAPTER 4 EFFECT OF GRAPHENE-ENHANCED COATINGS ON MARINE BIOFOULING

4.1 INTRODUCTION

Biofouling, which is composed of bacteria, diatoms, spores and larger marine organisms (algae, sponges, mussels, etc), occurs on solid surfaces that are immersed in seawater (Callow & Callow, 2011). The undesired colonization of marine organisms on submerged surfaces can increase surface roughness and drag resistance between surfaces and water, which leads to energy penalties, surface deterioration, the increase in fuel consumption and maintenance costs, and many other adverse impacts in marine industries (Callow & Callow, 2011; Bressy & Lejars, 2014; Lejars et al., 2012; Chambers et al., 2006). Therefore, antifouling coatings continue to emerge as a method to minimize the fouling on immersed surfaces. The main types of antifouling coatings include chemically active coating and non-toxic fouling release coatings (Bressy & Lejars, 2014).Chemically active coatings can control the colonizatio of marine organisms by releasing tin-free active compounds called biocides (Lejars et al., 2012),while fouling release coatings can inhibit the bacterial adhesion without chemical reactions as they do not contain biocides (Bressy & Lejars, 2014; Lejars et al., 2012; Gittens et al., 2013). Graphene based materials have been applied as enhanced anti-fouling coatings due to the superb anti-corrosion, antibacterial and hydrophobic properties (Lu et al., 2017; Nine et al., 2015; Krishnamoorthy et al., 2014).

The purpose of this study is to compare and assess the antifouling properties of two types of graphene-enhanced coatings by comparing the biofilm formation on the surface of polycarbonate coupons with no coatings and graphene-coated coupons.

4.2 MATERIALS AND METHODS

As shown in Figure 4.1 & Figure 4.2, three ARs were connected in parallel and fed with 100% filtered ocean water to imitate the marine environment. Each AR contained 20 coupons in an epoxy matrix, while the left two ARs contained 10 polycarbonate coupons coated with either Graphene Coat 111 (GC111) or Graphene Coat 112 (GC112) and 10 uncoated coupons, and the right AR contained 20 uncoated polycarbonate coupons. The coupons were coated by GIT with their graphene-enhanced coatings (a proprietary process).

Considering the high price of the graphene coatings, totally 20 GC111 and 20 GC112 coupons were ordered from GIT company and then divided into use in the two experiments. Therefore, AR1 and AR2 contained only 10 coated coupons.

Figure 4.1 Experimental set-up. AR1 (left) tested coupons with GC111 formula. AR2 (middle) tested coupons with GC112 formula. AR3(right) tested uncoated coupons.

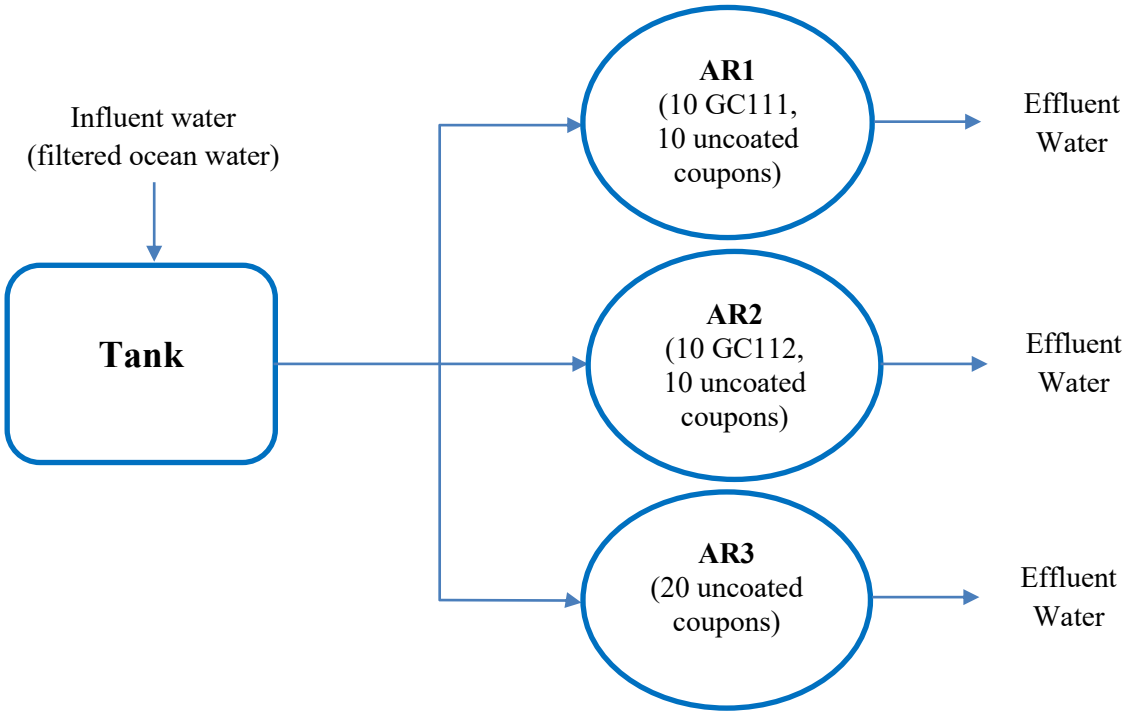

Figure 4.2. Schematic diagram of the experimental set-up.

The experimental conditions for this experiment are summarized in Table 4.1. As described in Chapter 3, the reactors, fittings, coupons and tubes were cleaned and sterilized before the experiments were performed.

Table 4.1. Summary of the experimental conditions.

AR rotational speed (rpm)	60
Water flow (mL/min)	7.83
Water temperature	Room temperature (20 ℃)
Water	100% filtered ocean water from Dalhousie Aquatron Centre

The reactors were covered with aluminum foil to prevent phototrophic bacterial growth. After an acclimation period of 2-weeks, two coupons were removed from each AR for sampling. For AR1 and AR2, one graphene-enhanced coupon and one uncoated coupon were removed, while for AR3, two uncoated polycarbonate coupons were taken out and sampled for biofilm recovery and analysis. Biological parameters such as tATP, HPC and EPS were quantified for ten weeks to assess the antifouling performance between the graphene-based coupons and uncoated coupons.

4.3 RESULTS AND DISCUSSION

4.3.1 Influent Water

The influent water used in this experiment was 100% filtered ocean water, collected from the Dalhousie Aquatron Centre during January 2021 and April 2021. The water was sampled and analyzed every week for pH, turbidity and cATP. The results are summarized in Table 4.2.

Table 4.2. Average water quality conditions measured from the influent water.

Parameter	***Mean***	***n***
pH	*7.7 ± 0.1*	*9*
Turbidity (NTU)	*0.5 ± 1.5*	*9*
cATP (pg cATP mL^{-1})	*990± 930*	*9*
Experimental Period	*January 2021 – April 2021*	

Figure 4.3 shows the water quality of influent during the 9 weeks.The fluctuation of the water quality parameters can be attributed to nutrient, temperature changes and seasonality from the filtered ocean water collected from the Dalhousie Aquatron Centre. The marine fouling behaviour can be affected by the differences in seawater temperature and daylight irradiation, which may contribute to the fluctuated cATP concentrations (Nurioglu et al., 2015).

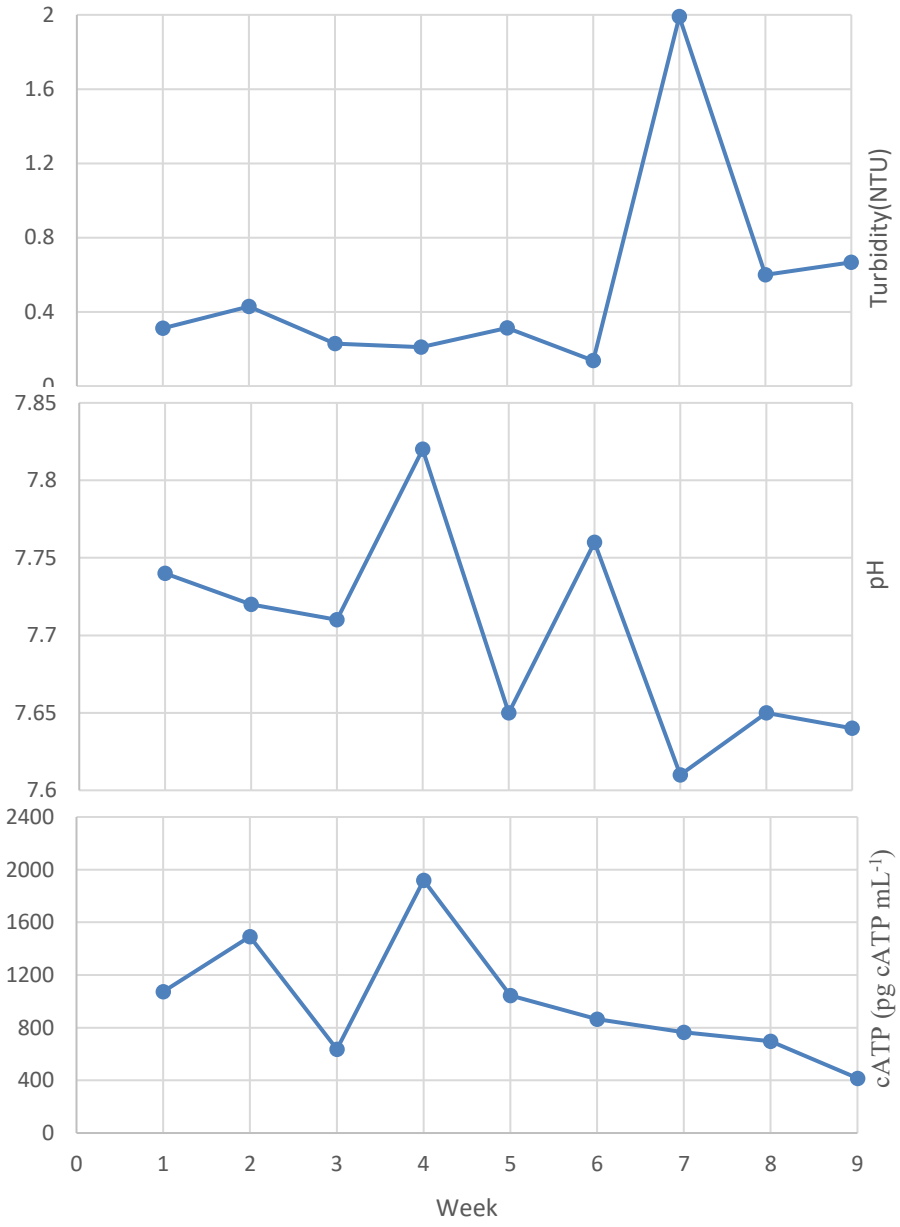

Figure 4.3 Influent water quality summary: cATP; Turbidity; pH.

4.3.2 Biofilm Accumulation Comparison

Biofilm ATP was tested on the surface of graphene-based coupons and uncoated coupons

for 9 weeks to compare the biofilm accumulation. As shown in Figure 4.4, the biofilm accumulated steadily on both graphene-enhanced coupons in the first five weeks, with a decrease in tATP concentrations in the following 4 weeks. The tATP concentrations of uncoated coupons almost kept the same during the 9 weeks.

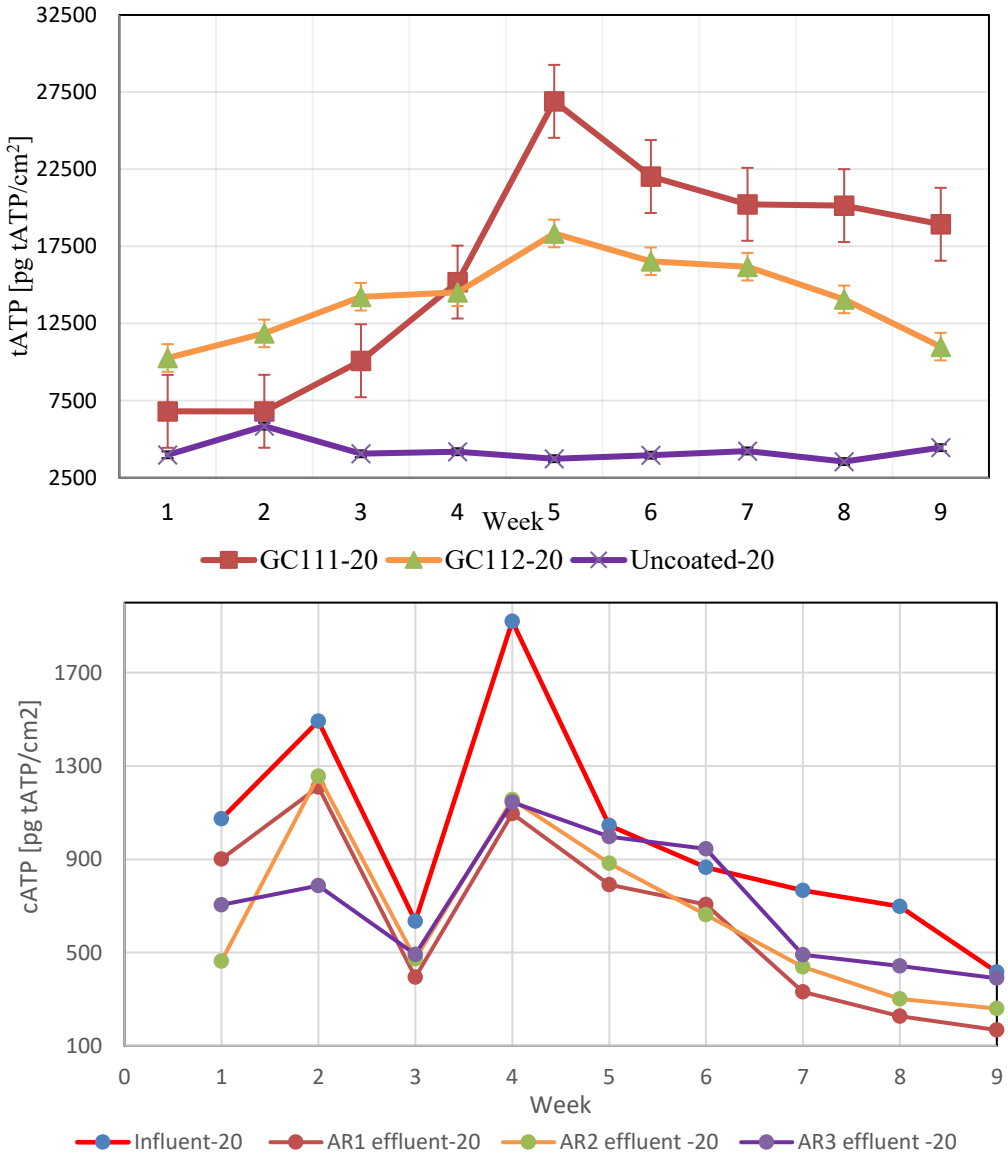

Figure 4.4. Biofilm tATP concentrations (top) from the graphene- based coupons and uncoated coupons and aqueous cATP (bottom) of the influent and effluent from the three Ars.

In terms of the biomass accumulated on the surface of the coatings, the mean tATP values for the GC111, GC112 and uncoated coupons correspond to a concentration of 16000±9500,

$1.4\times10^4\pm4.2\times10^3$, $4.2\times10^3\pm1.5\times10^3$ pg tATP/cm^2, respectively. Graphene-enhanced coupons accumulated significantly more biomass than the uncoated coupons, which may be attributed to the hydrophobic surface of graphene coatings, as microorganisms can attach more rapidly to non-polar and hydrophobic surfaces compared with hydrophilic surfaces (Holland et al., 2004). According to Lejars et al. (2012), the settlement of marine fouling can be influenced by salinity, nutrient levels, pH, temperature, etc.. Consequently, the declined cATP concentration in influent water after week 4 may be one of the reasons for the decrease of biofilm tATP concentrations of graphene coatings.

Regardless of the fluctuations of cATP concentrations, it is obvious that the aqueous ATP concentration from each AR effluent water was lower than that in the influent water and the gap was more obvious between the effluent water from ARs housing graphene-coated coupons and influent water. This could be explained by the antibacterial capability of graphene. The antimicrobial activity of GO can be ascribed to both physical and chemical interactions, including cell membrane disruption and oxidative stress (Chen et al., 2014). The cell membrane can be penetrated by the atomically sharp edges of graphene, and the lipid peroxidation due to the oxidative stress of GO can cause membrane damage (Chen et al., 2014; Perreault et al., 2015; Akhavan et al., 2010; Krishnamoorthy et al., 2012).

In addition, The HPC was analyzed to further compare the difference in biofilm accumulation on graphene-coated coupons and uncoated coupons (Figure 4.5). The average HPC recovered from the GC11-coated coupons, GC112-coated coupons and uncoated coupons, were $3.3\times10^5\pm3.1\times10^5$, $3.0\times10^5\pm2.6\times10^5$ and $5.2\times10^3\pm3.5\times10^3$ CFU/cm^2, respectively. As shown in Figure 4.5, a significantly higher amount of viable bacterial cells were accumulated on the graphene-coated coupons, which corresponds to a similar result as that of tATP analysis. However, it is important to note that this method only detects the culturable component of biofilm-bound bacteria.

.

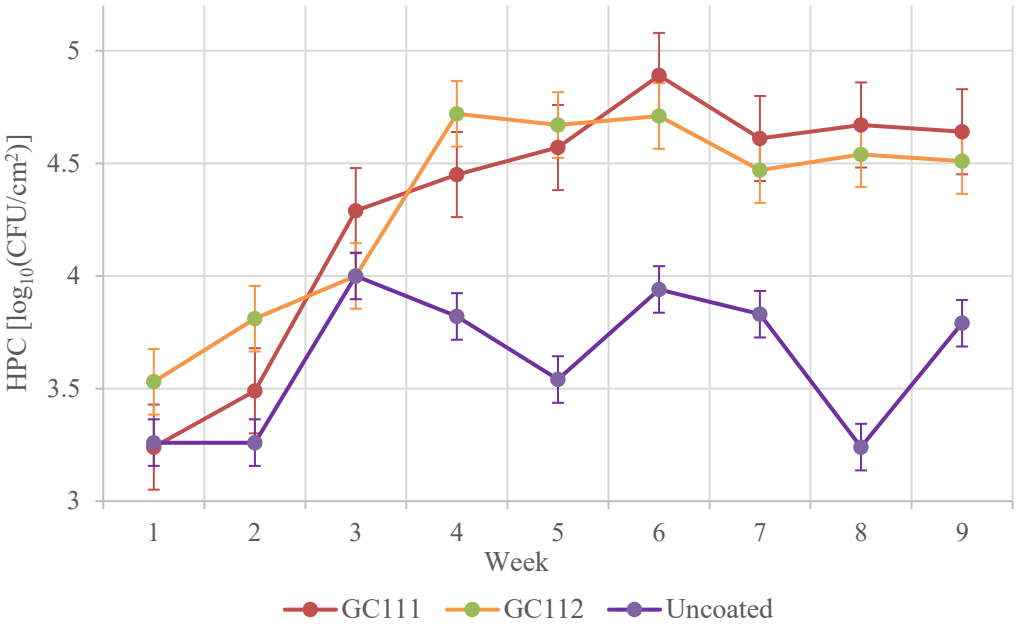

Figure 4.5. Average heterotrophic plate counts from biofilm-bound bacteria recovered from the coupons: GC111, GC112, and uncoated ones.

4.3.3 EPS Formation

Extra Polymeric Substances is primarily composed of carbohydrates and proteins, which provides architectural structure and mechanical stability to the attached biomass (Allison, 2003; Flemming & Wingender, 2010). Figure 4.6 summarized the protein and carbohydrate fractions quantified from EPS matrix on the three coatings. The mean concentrations for the carbohydrate fractions were 549±121, 535±76 and 488±32 µg glucose/cm^2 recovered from the surface of GC111, GC112 and uncoated coupons, respectively. The mean protein concentrations tested from the biofilm formed on GC111, GC112 and uncoated coupons were 80±51, 61±28 and 47±29µg BSA/cm^2, respectively. Both the carbohydrate concentrations and protein concentration from the biofilm extracted on the graphene coatings were higher than those on the uncoated coupons, and there was a significant increase of the protein fraction recovered from the graphene coated coupons from week 6 to week 9. This would improve the formation and stabilization of the EPS matrix as the proteins and carbohydrates can resist antimicrobial agents such as antibiotics and disinfectants (Allison, 2003; Flemming & Wingender, 2010) .

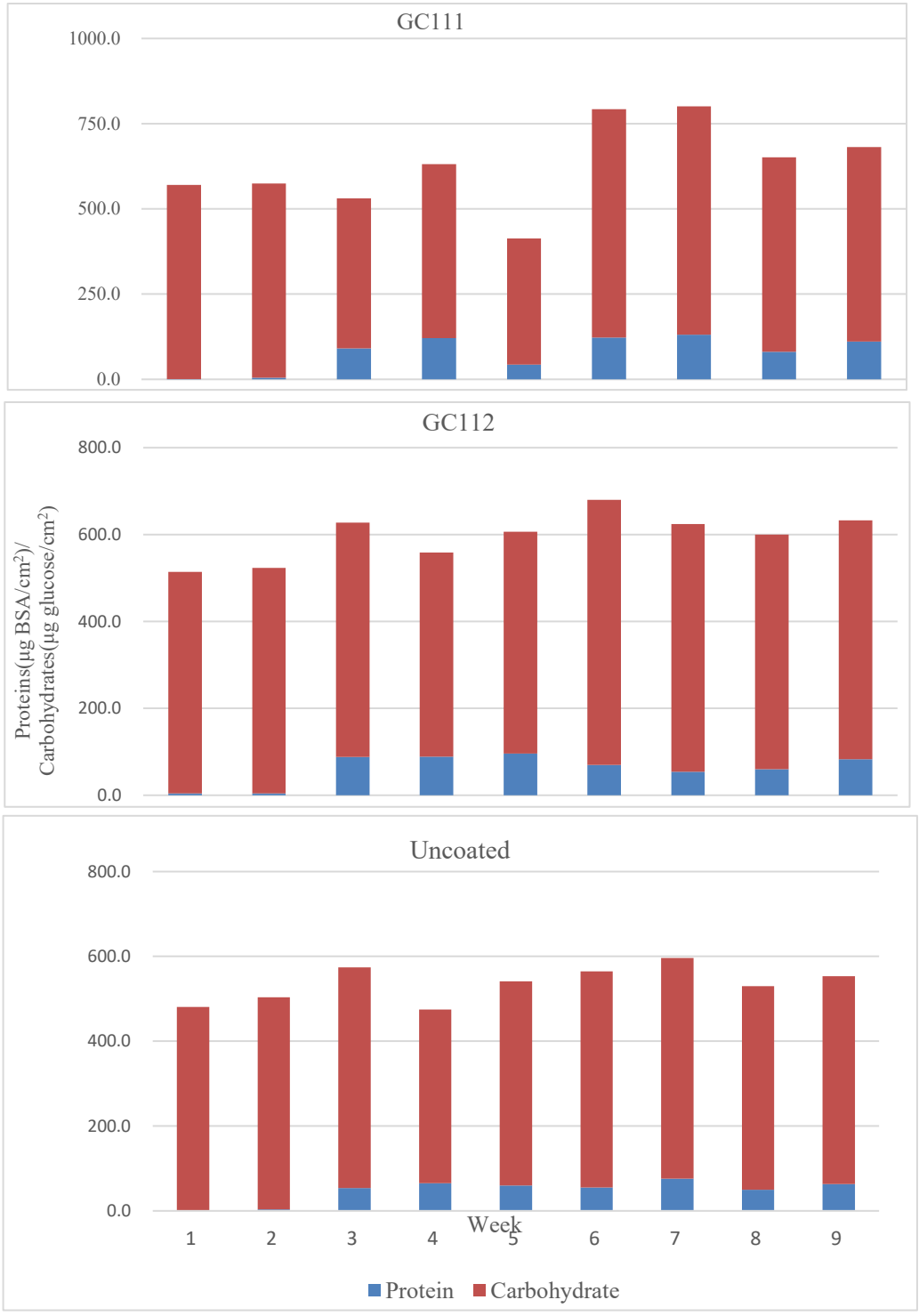

Figure 4.6. Average Carbohydrate and protein concentration in the EPS matrix.

4.4 CONCLUSIONS

A bench-scale experiment was implemented with ARs and filtered ocean water to assess the antifouling performance of graphene-enhanced coatings. The main findings of this section include:

● Graphene-enhanced coatings accumulated significantly higher amout of biomass than uncoated ones, which may be attributed to the hydrophobic surface of graphene coatings and the material composition of the coatings.

● The cATP concentrations in all effluent water from ARs housing graphene-coated coupons were much lower than that in the influent water, mainly due to the antibacterial property of graphene.

●Both the carbohydrate concentrations and protein concentration from the biofilm extracted on the graphene coatings were higher than those on the uncoated coupons, which would assist the formation and stabilization of the EPS matrix.

CHAPTER 5 EFFECT OF WATER TEMPERATURE ON MARINE BIOFOULING

5.1 INTRODUCTION

Water temperature is a major factor in biofilm development and growth as it can modify hydrophobicity and microbial cell surface charge (Van Loosdrecht et al., 1990). However, it is hard to figure out the effects of water temperature on bacterial cell attachment, as different bacteria show different adhesion performances at different water temperature. The water temperature can change the bacterial community composition and affect the EPS (Lindström et al., 2005; Morimatsu et al., 2012). It has been proven that higher water temperature would decrease the EPS matrix viscosity (Lewis et al., 1989).According to previous studies, the enzymatic activities of bacterial cells for the degradation of organic matter would be stimulated under warmer conditions, thus increasing bacterial biofilm biomass (Brown et al., 2004; Amthor, 1984). However, it was also studied that the bacterial growth efficiency might decrease at higher water temperature over a longer period (Ratkowsky et al., 1982; Sand-Jensen et al., 2007).

The objective of this section is to assess the effect of water temperature on biofilm growth by comparing the biofilm formation on the surface of coupons submerged in marine water of different water temperature.

5.2 MATERIALS AND METHODS

As shown in Figure 5.1 & Figure 5.2, three ARs were connected in parallel and fed with 100% filtered ocean water to imitate the marine environment. The set-up of the three ARs was the same of that in Chapter 4. The influent water flowed through a capsule filter (size: 25μm) first, then heated to 35℃ and finally flowed into the ARs.

Figure 5.1 Experimental set-up.

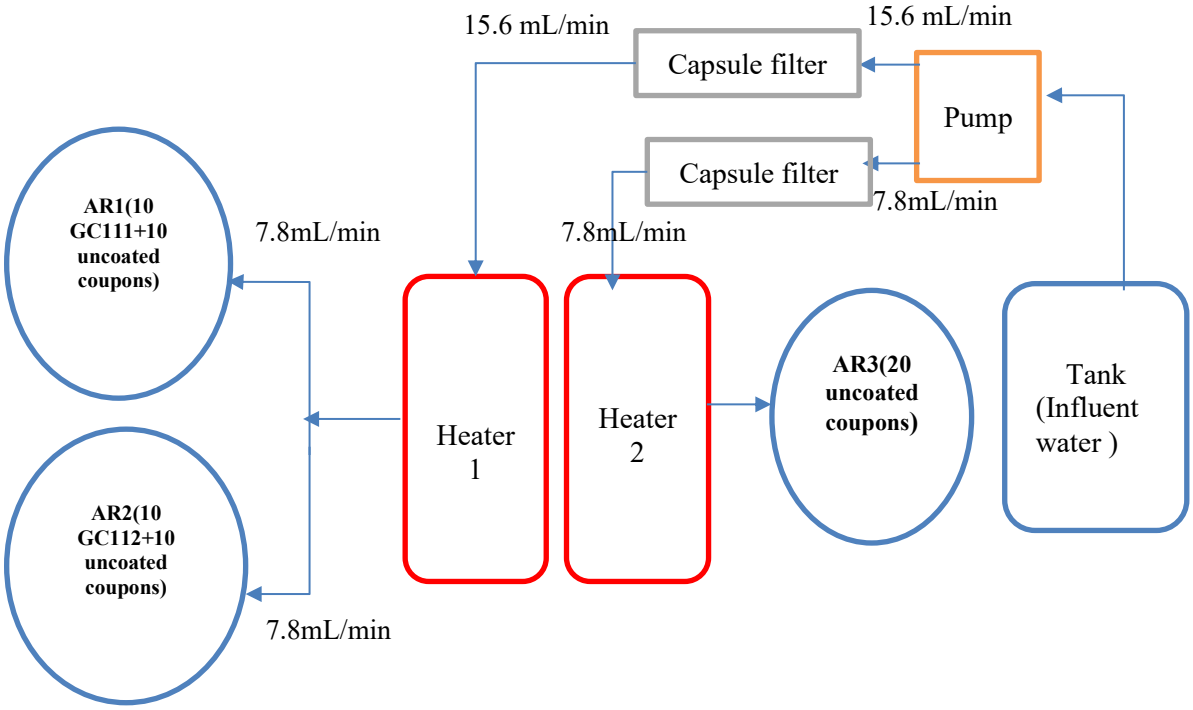

Figure 5.2. Schematic diagram of the experimental arrangement.

The conditions for this series of experiments are summarized in Table 4.1. As described in Chapter 3, the reactors, fittings, coupons and tubes were cleaned and sterilized before the experiment operation. The reactors were operated at a rotational speed of 60 rpm and a flow

rate of 7.83 mL/min to achieve a simulating shear stress of 0.15 N/m^2 and a hydraulic retention time of 2 hours. As Heater 1 provided heated water for both AR1 and AR2, the flow rate was adjusted to 15.6 mL/min through the use of peristaltic pumps. The heated water from Heater1 was then divided equally into two flows to feed AR1 and AR2, which corresponded to a flow rate of 7.8 mL/min of each. As Dalhousie Aquatron Center stopped providing ocean water at this point in the study, the ocean water was collected locally from Point Pleasant Park instead from April to July in 2021, and then capsule filter was used to filter the collected water. The pore size of the capsule filter was the same as that in the Dalhousie Aquatron Centre, that was 25 μm.

Table 5.1. Summary of the experimental conditions.

AR rotational speed (rpm)	60
Water flow (mL/min)	7.83
Water temperature	35 ℃
Water	ocean water from Point Pleasant Park

The reactors were covered with aluminum foil to prevent phototrophic bacterial growth. After an acclimation period of 2 weeks, two coupons were removed from each AR for sampling. For AR1 and AR2, one graphene-enhanced coupon and one uncoated coupon were removed, while for AR3, two uncoated polycarbonate coupons were taken out and sampled for biofilm recovery and analysis. Biological parameters such as tATP, HPC and EPS were quantified for ten weeks to assess the antifouling performance between the graphene-based coupons and uncoated coupons.

5.3 RESULTS AND DISCUSSION

5.3.1 Influent Water

The influent water used in this experiment was ocean water collected from Point Pleasant Park. The water was sampled and characterized every week at the intake reservoirs for general water quality parameters including cATP concentrations. The results are summarized in Table 5.2.

Table 5.2. Average water quality conditions measured from the influent water.

Parameter	***Mean***	***n***
pH	*7.62 ± 0.14*	*10*
Turbidity (NTU)	*0.52 ± 0.33*	*10*
cATP (pg cATP mL^{-1})	*438± 198*	*10*
Experimental Period	*April 2021 – July 2021*	

Compared to the filtered ocean water from Dalhousie Aquantron Centre, the turbidity and pH of these two sources of influent water were almost the same, while the cATP concentrations of filtered water from Point Pleasant Park were obviously lower than those of water from Dalhousie Aquantron Centre. Regardless of the influence of water temperature, the biofilm mass accumulated on coupons in this study should be considered less than that of the previous study.

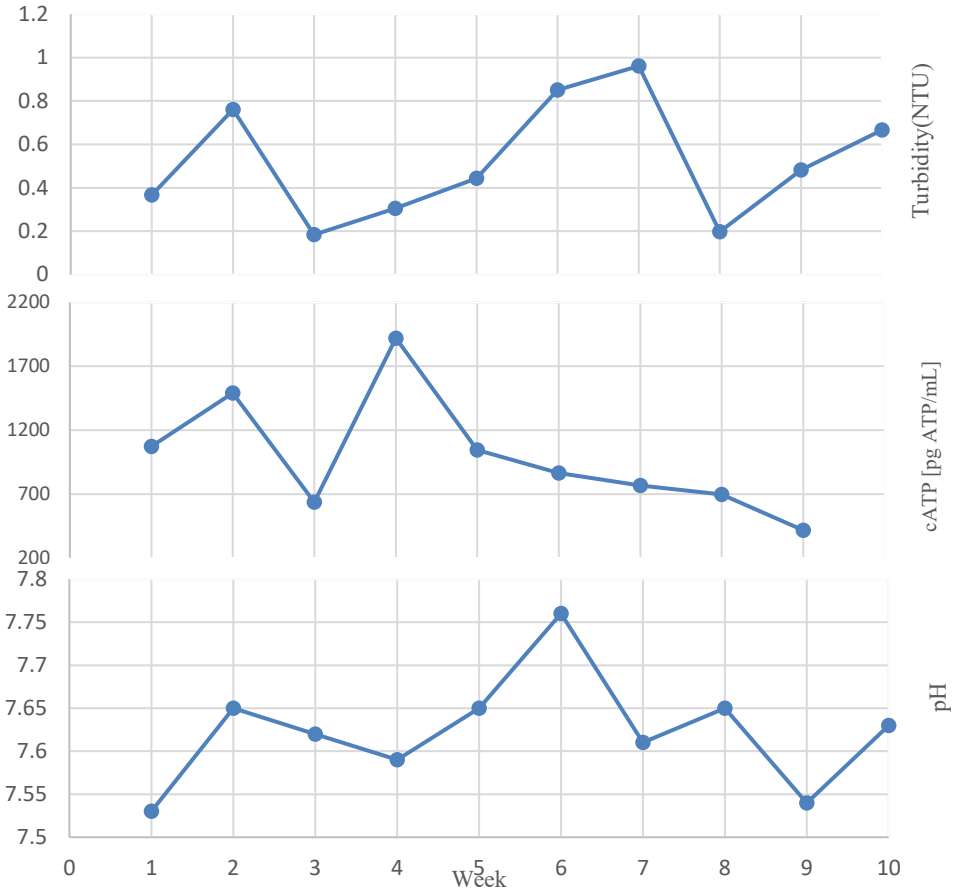

Figure 5.3. Influent water quality summary: cATP; Turbidity; pH.

5.3.2 Biofilm Accumulation Comparison

Biofilm ATP was tested on the surface of graphene-based coupons and uncoated coupons for 9 weeks to compare the biofilm accumulation. To assess the impact of water temperature on marine biofouling, tATP concentrations of GC111, GC112 and uncoated coupons in both room temperature and 3℃ of water were compared.

As shown in Figure 5.4, the biofilm accumulated steadily on both graphene-enhanced coupons in the first 4 weeks, with a decrease in tATP concentrations in the following 5 weeks. The tATP concentrations of uncoated coupons remained almost the same during the 9 weeks; solid lines represent the tATP concentration of coatings in water of room temperature, and the dashed lines represent the tATP concentration of coating in water at

35 ℃.

In terms of the biomass accumulated on the surface of the coatings submerged in the ocean water at 35 ℃, the mean tATP values for the GC111, GC112 and uncoated coupons correspond to concentrations of $2.4\times10^4\pm9.2\times10^3$, $2.2\times10^4\pm2.1\times10^4$, $1.5\times10^3\pm1.2\times10^3$ pg tATP/cm^2, respectively.

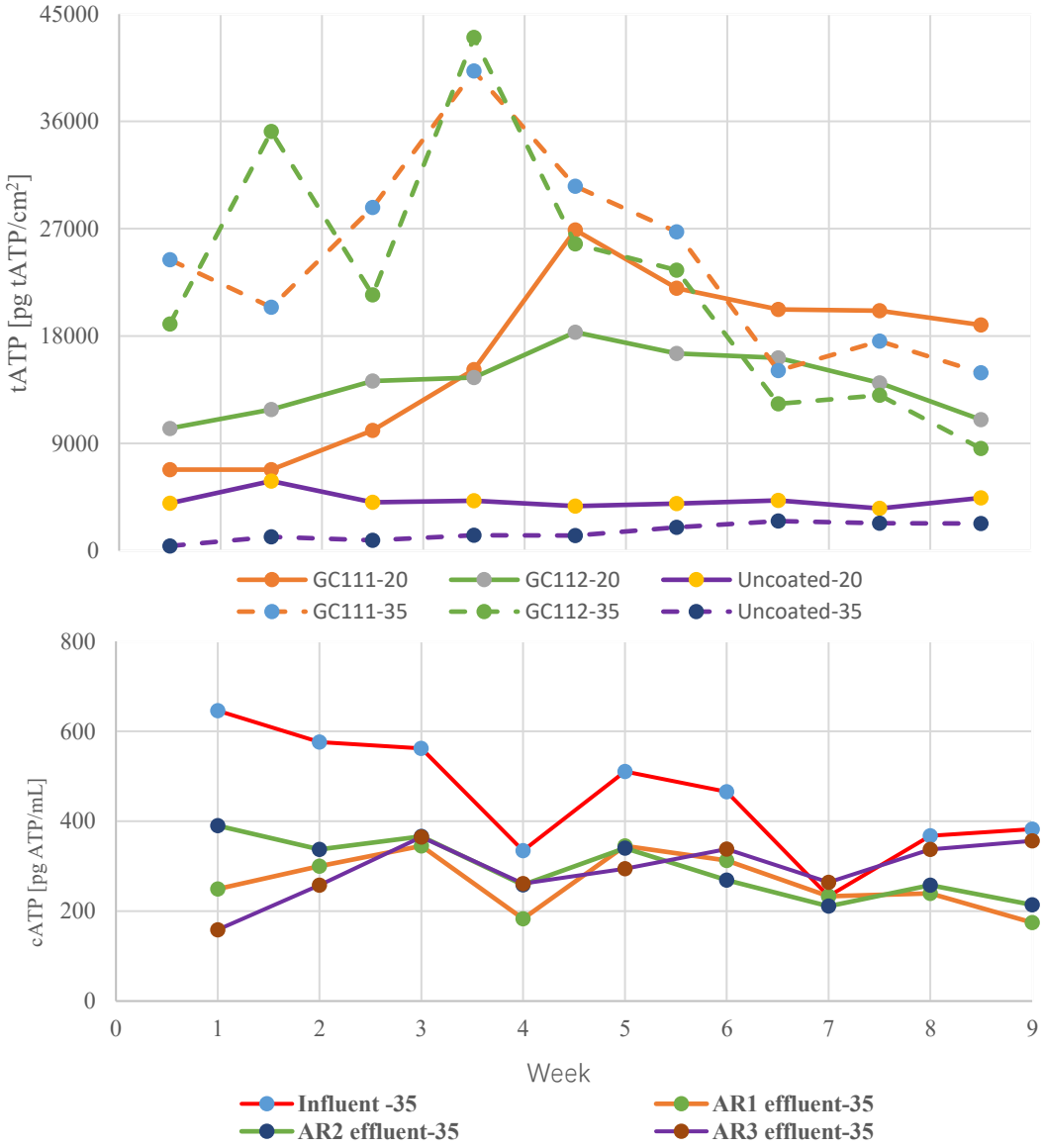

Figure 5.4. Biofilm tATP concentrations (top) from the graphene- based coupons and uncoated coupons and aqueous cATP (bottom) of the influent and effluent from the three Ars.

Biofilm formation was faster, and microbial colonization of the substratum occurred earlier, when the temperature of flowing water was increased. Despite the lower cATP concentrations of warmer water, the graphene-based coupons accumulated a larger amount

of biomass on the surface in the water at higher temperature during the first 4 weeks. However, from week 4 to week 9, the tATP concentrations of coupons in warmer water decreased rapidly. This could be attributed to the stimulating impact of higher water temperature on bacterial growth and metabolism (Brown et al., 2004; Amthor, 1984). The increase in bacterial biofilm biomass and activity under high-temperature conditions is valid in the exponential bacterial growth phase. After the maximum bacterial growth, it would be nutrient limited and the bacterial growth efficiency may decline, which leads to less biomass (del Giorgio & Cole, 1998). In addition, the final tATP concentrations of coatings in warmer water decreased to values less than those in water at nominally room temperature(around 20 ℃), which may prove that the temperature would not affect the final biomass of the bio film. Putting this another way, the biofilm carrying capacity under the two temperature conditions was similar (Villanueva et al., 2010).

Furthermore, under conditions of higher water temperature, the aqueous ATP concentration from each AR effluent water was also lower than that in the influent water. However, the difference between the cATP concentrations in effluent water from ARs housing graphene-coated coupons and those in effluent water from ARs housing uncoated coupons was smaller. This was because that the water temperature could modify hydrophobicity and microbial cell surface charge, thus affecting initial cell attachment.

As shown in Figure 5.5. The average HPC recovered from the GC11-coated coupons , GC112-coated coupons and uncoated coupons, were $4.1\times10^5\pm3.9\times10^5$, $2.5\times10^5\pm2.4\times10^5$, $5.2\times10^3\pm7.3\times10^3$ CFU/cm^2, respectively. As shown in Figure 5.5, a significantly higher amount of viable bacterial cells were accumulated on the graphene-coated coupons in warmer water in the first 4 weeks, and then decreased rapidly during the following 5 weeks, which corresponds to a similar result as that of tATP analysis. However, it is important to note that this method only detects the culturable component of biofilm-bound bacteria.

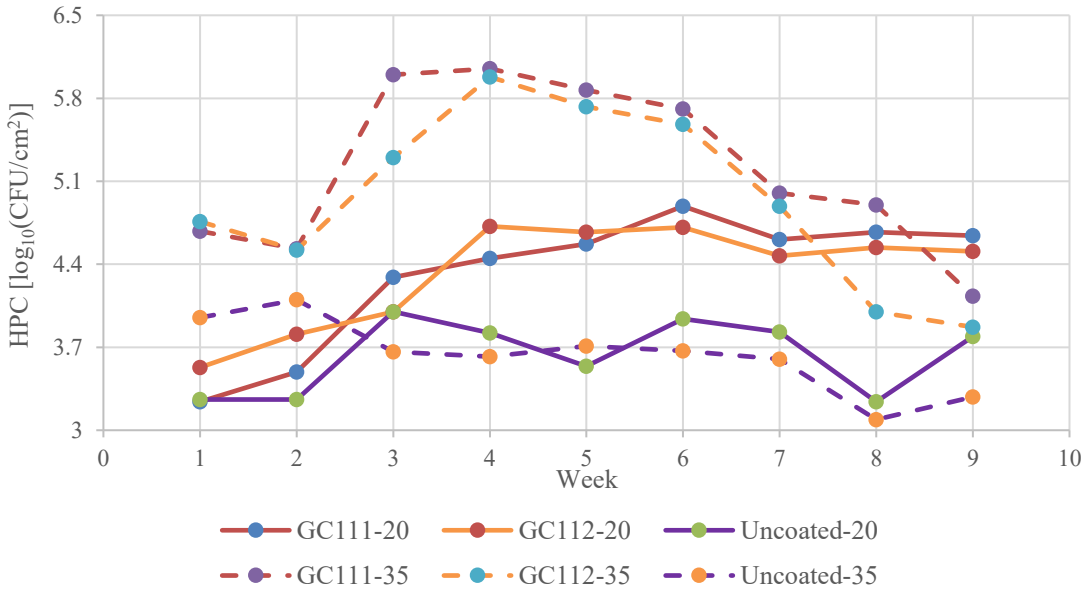

Figure 5.5. Average heterotrophic plate counts from biofilm-bound bacteria recovered from the coupons: GC111, GC112 and uncoated ones

5.3.3 EPS Formation

Figure 5.6 summarized the protein and carbohydrate fractions quantified from the EPS matrix on the three coatings. Under the condition of higher water temperature, the mean concentrations for the carbohydrate fractions were 510±142, 478±114 and 454±83 µg glucose/cm2 recovered from the surface of GC111, GC112 and uncoated coupons, respectively. The mean protein concentrations tested from the biofilm formed on GC111, GC112 and uncoated coupons were 67±58, 63±45 and 49±41 µg BSA/cm2, respectively. Both the carbohydrate concentrations and protein concentration from the biofilm extracted on the graphene coatings were higher than those on the uncoated coupons. By comparing the EPS formation of biofilm recovered from coupons in water of room temperature with that of biofilm recovered from coupons in higher water temperature, both protein and carbohydrate concentrations were increased earlier and more significantly in the first 4 weeks, with an obvious decrease in the following five weeks. The final concentrations of protein and carbohydrate from coatings in higher water temperature were lower than that in room water temperature. The reason was that water temperature could affect the EPS

and the EPS matrix viscosity would be decreased under warmer conditions(Lewis et al., 1989; Morimatsu et al., 2012).

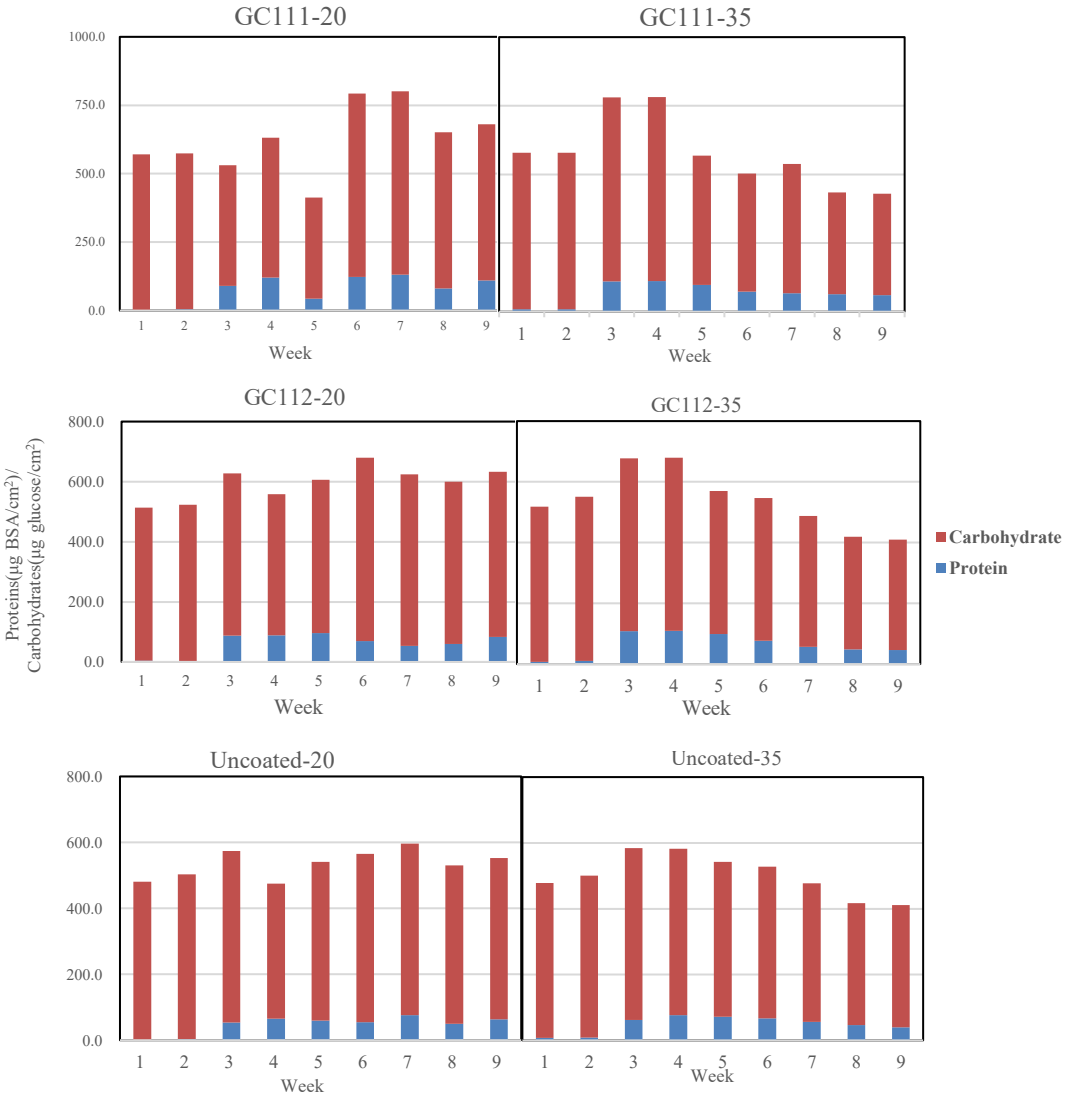

Figure 5.6. Average Carbohydrate and protein concentration in the EPS matrix (water temperature: 20 ℃ (left); 35 ℃ (right)).

5.4 CONCLUSIONS

A bench-scale experiment was implemented with ARs and heated filtered ocean water to assess the effect of water temperature on marine biofouling. The main findings of this section include:

● Biofilm formation is faster, and microbial colonization of the substratum occurs earlier, when the temperature of flowing water is increased. However, after the maximum bacterial growth, the rate of the bacterial growth would decline, which leads to less biomass in a long period.

● The water temperature could modify hydrophobicity and microbial cell surface charge, thus affecting initial cell attachment.

●The concentrations of protein and carbohydrate from coatings in higher water temperature were lower than that in room temperature water, as the water temperature could affect EPS and the EPS matrix viscosity would be decreased at higher water temperature.

CHAPTER 6 CONCLUSIONS

6.1 CONCLUSIONS

This research was divided into two experiments to assess the antifouling performance of graphene-enhanced coatings and the effect of water temperature on biomass growth. The antibacterial property of graphene was proved in Experiment 1, and the higher amount of biomass accumulated on graphene coated coupons might be ascribed to material composition and hydrophobic surface of graphene coatings. In Experiment 2, it was verified that higher water temperature could accelerate biofilm formation at the beginning , while the bacterial growth would be slower in a longer period compered to that under colder condition.

6.2 RECOMMENDATIONS

To improve the performance of graphene coatings, more attention can be paid to the composition and the hydrophobic properties of the graphene coatings to assess the antifouling performance. In addition, it is recommended to widen the water temperature range of the second experiment to further investigate the effects of water temperature on biofouling.

REFERENCES

Allison, D. G. (2003). The biofilm matrix. *Biofouling*, *19*(2), 139–150. https://doi.org/10.1080/0892701031000072190

Amthor, J. S. (1984). The role of maintenance respiration in plant growth. *Plant, Cell and Environment*, *7*(8), 561–569. https://doi.org/10.1111/1365-3040.ep11591833

Akhavan, O., & Ghaderi, E. (2010). Toxicity of graphene and graphene oxide Nanowalls against bacteria. *ACS Nano*, *4*(10), 5731–5736. https://doi.org/10.1021/nn101390x

Balakrishnan, A., Jena, G., Pongachira George, R., & Philip, J. (2020). Polydimethylsiloxane–graphene oxide nanocomposite coatings with improved anti-corrosion and anti-biofouling properties. Environmental Science and Pollution Research, 28(6), 7404–7422. https://doi.org/10.1007/s11356-020-11068-5

Bressy, C., & Lejars, M. (2014). Marine Fouling: An Overview. *Journal of Ocean Technology 9(4):19-28.*

Brown, J. H., Gillooly, J. F., Savage, V. M., & West, G. B. (2004). Toward a metabolic theory of ecology. *Ecology*, *85*(7), 1771–1789. https://doi.org/10.1890/03-9000

Callow, J. A., & Callow, M. E. (2011). Trends in the development of environmentally friendly fouling-resistant marine coatings. *Nature Communications*, *2*(1). https://doi.org/10.1038/ncomms1251

Chambers, L. D., Stokes, K. R., Walsh, F. C., & Wood, R. J. K. (2006). Modern approaches to marine antifouling coatings. *Surface and Coatings Technology*, *201*(6), 3642–3652. https://doi.org/10.1016/j.surfcoat.2006.08.129

Chen, J., Peng, H., Shao, F., Yuan, Z., & Han, H. (2014). Graphene oxide exhibits broad-spectrum antimicrobial activity against bacterial phytopathogens and fungal conidia by intertwining and membrane perturbation. *Nanoscale*, *6*(3), 1879–1889. https://doi.org/10.1039/c3nr04941h

Cheng, W., Lu, X., Kaneda, M., Zhang, W., Bernstein, R., Ma, J., & Elimelech, M. (2019). Graphene oxide-functionalized membranes: The importance of nanosheet surface exposure for biofouling resistance. *Environmental Science & Technology*, *54*(1), 517–526. https://doi.org/10.1021/acs.est.9b05335

Giorgio, P. A., & Cole, J. J. (1998). Bacterial growth efficiency in Natural Aquatic Systems. *Annual Review of Ecology and Systematics*, *29*(1), 503–541. https://doi.org/10.1146/annurev.ecolsys.29.1.503

Farhat, N. M., Vrouwenvelder, J. S., Van Loosdrecht, M. C. M., Bucs, S. S., & Staal, M. (2016). Effect of water temperature on biofouling development in reverse osmosis membrane systems. *Water Research*, *103*, 149–159. https://doi.org/10.1016/j.watres.2016.07.015

Flemming, H.-C., & Wingender, J. (2010). The biofilm matrix. *Nature Reviews Microbiology*, *8*(9), 623–633. https://doi.org/10.1038/nrmicro2415

Gagnon, G. A., & Slawson, R. M. (1999). An efficient biofilm removal method for bacterial cells exposed to drinking water. *Journal of Microbiological Methods*, *34*(3), 203–214. https://doi.org/10.1016/s0167-7012(98)00089-x

Georgakilas, V., Bourlinos, A. B., Chandra, V., Kim, N., Kemp, K. C., Hobza, P., Zboril, R., & Kim, K. S. (2012). Functionalization of graphene: Covalent and non-covalent approaches, derivatives and applications. *Chemical Reviews*, *112*(11), 6156–6214. https://doi.org/10.1021/cr3000412

Gittens, J. E., Smith, T. J., Suleiman, R., & Akid, R. (2013). Current and emerging environmentally-friendly systems for fouling control in the Marine Environment. *Biotechnology Advances*, *31*(8), 1738–1753. https://doi.org/10.1016/j.biotechadv.2013.09.002

Holland, R., Dugdale, T. M., Wetherbee, R., Brennan, A. B., Finlay, J. A., Callow, J. A., & Callow, M. E. (2004). Adhesion and motility of fouling diatoms on a silicone elastomer. *Biofouling*, *20*(6), 323–329. https://doi.org/10.1080/08927010400029031

Krishnamoorthy, K., Veerapandian, M., Zhang, L.-H., Yun, K., & Kim, S. J. (2012). Antibacterial efficiency of graphene nanosheets against pathogenic bacteria via lipid peroxidation. *The Journal of Physical Chemistry C*, *116*(32), 17280–17287. https://doi.org/10.1021/jp3047054

Krishnamoorthy, K., Jeyasubramanian, K., Premanathan, M., Subbiah, G., Shin, H. S., & Kim, S. J. (2014). Graphene oxide nanopaint. *Carbon*, *72*, 328–337. https://doi.org/10.1016/j.carbon.2014.02.013

Lewis, S. (1989). Factors influencing the detachment of a polymer-associated Acinetobacter sp. from stainless steel. *International Journal of Food Microbiology*, *8*(2), 155–164. https://doi.org/10.1016/0168-1605(89)90070-6

Lindström E. S., Kamst-Van Agterveld, M. P., & Zwart, G. (2005). Distribution of typical freshwater bacterial groups is associated with ph, temperature, and lake water retention time. *Applied and Environmental Microbiology*, *71*(12), 8201–8206. https://doi.org/10.1128/aem.71.12.8201-8206.2005

Lu, X., Feng, X., Werber, J. R., Chu, C., Zucker, I., Kim, J.-H., Osuji, C. O., & Elimelech, M. (2017). Enhanced antibacterial activity through the controlled alignment of graphene oxide nanosheets. *Proceedings of the National Academy of Sciences*, *114*(46). https://doi.org/10.1073/pnas.1710996114

Manderfeld, E., Kleinberg, M. N., Thamaraiselvan, C., Koschitzki, F., Gnutt, P., Plumere, N., Arnusch, C. J., & Rosenhahn, A. (2021). Electrochemically activated laser-induced graphene coatings against marine biofouling. *Applied Surface Science*, *569*, 150853. https://doi.org/10.1016/j.apsusc.2021.150853

Morimatsu, K., Eguchi, K., Hamanaka, D., Tanaka, F., & Uchino, T. (2012). Effects of temperature and nutrient conditions on biofilm formation of pseudomonas putida. *Food Science and Technology Research*, *18*(6), 879–883. https://doi.org/10.3136/fstr.18.879

Nine, M. J., Cole, M. A., Tran, D. N., & Losic, D. (2015). Graphene: A multipurpose material for protective coatings. *Journal of Materials Chemistry A*, *3*(24), 12580–12602.

https://doi.org/10.1039/c5ta01010a

Nurioglu, A. G., Esteves, A. C., & de With, G. (2015). Non-toxic, non-biocide-release antifouling coatings based on molecular structure design for Marine Applications. *Journal of Materials Chemistry B*, *3*(32), 6547–6570. https://doi.org/10.1039/c5tb00232j

Park, S. K., Kim, Y. K., Oh, Y. S., & Choi, S. C. (2015). Growth kinetics and chlorine resistance of heterotrophic bacteria isolated from young biofilms formed on a model drinking water distribution system. *Korean Journal of Microbiology*, *51*(4), 355– 363. https://doi.org/10.7845/kjm.2015.5050

Perreault, F., de Faria, A. F., Nejati, S., & Elimelech, M. (2015). Antimicrobial properties of graphene oxide nanosheets: Why size matters. *ACS Nano*, *9*(7), 7226–7236. https://doi.org/10.1021/acsnano.5b02067

Pintar, K. D. M., & Slawson, R. M. (2003). Effect of temperature and disinfection strategies on ammonia-oxidizing bacteria in a bench-scale drinking water distribution system. *Water Research*, *37*(8), 1805–1817. https://doi.org/10.1016/S0043-1354(02)00538-9

Pompermayer, D. M. C., & Gaylarde, C. C. (2000). The influence of temperature on the adhesion of mixed cultures of Staphylococcus aureus and escherichia coli to polypropylene. *Food Microbiology*, *17*(4), 361–365. https://doi.org/10.1006/fmic.1999.0291

Ratkowsky, D. A., Olley, J., McMeekin, T. A., & Ball, A. (1982). Relationship between temperature and growth rate of bacterial cultures. *Journal of Bacteriology*, *149*(1), 1–5. https://doi.org/10.1128/jb.149.1.1-5.1982

Salta, M., Wharton, J. A., Blache, Y., Stokes, K. R., & Briand, J.-F. (2013). Marine biofilms on artificial surfaces: Structure and Dynamics. *Environmental Microbiology*. https://doi.org/10.1111/1462-2920.12186

Saur, T., Morin, E., Habouzit, F., Bernet, N., & Escudié, R. (2017). Impact of wall shear stress on initial bacterial adhesion in rotating annular reactor. PLOS ONE, 12(2). https://doi.org/10.1371/journal.pone.0172113

Rosenhahn, A., Schilp, S., Kreuzer, H. J., & Grunze, M. (2010). The role of "inert" surface chemistry in marine biofouling prevention. *Physical Chemistry Chemical Physics*, *12*(17), 4275. https://doi.org/10.1039/c001968m

SAND-JENSEN, K. A. J., PEDERSEN, N. I. E. L. S. L. A. G. E. R. G. A. A. R. D., & SØNDERGAARD, M. O. R. T. E. N. (2007). Bacterial metabolism in small temperate streams under contemporary and future climates. *Freshwater Biology*, *52*(12), 2340–2353. https://doi.org/10.1111/j.1365-2427.2007.01852.x

Shao, S., Shi, D., Li, Y., Liu, Y., Lu, Z., Fang, Z., & Liang, H. (2019). Effects of water temperature and light intensity on the performance of gravity-driven membrane system. *Chemosphere*, *216*, 324–330. https://doi.org/10.1016/j.chemosphere.2018.10.156

Van Loosdrecht, M. C. M., Norde, W., & Zehnder, A. J. B. (1990). Physical Chemical Description of bacterial adhesion. *Journal of Biomaterials Applications*, *5*(2), 91–106. https://doi.org/10.1177/088532829000500202

Villanueva, V. D., Font, J., Schwartz, T., & Romaní, A. M. (2010). Biofilm Formation at warming temperature: Acceleration of microbial colonization and microbial interactive effects. *Biofouling*, *27*(1), 59–71. https://doi.org/10.1080/08927014.2010.538841

Yang, W. J., Neoh, K.-G., Kang, E.-T., Teo, S. L.-M., & Rittschof, D. (2014). Polymer brush coatings for combating marine biofouling. *Progress in Polymer Science*, *39*(5), 1017–1042. https://doi.org/10.1016/j.progpolymsci.2014.02.002

Zhu, Y., Wang, H., Li, X., Hu, C., Yang, M., & Qu, J. (2014). Characterization of biofilm and corrosion of cast iron pipes in drinking water distribution system with UV/Cl2 disinfection. *Water Research*, *60*, 174–181. https://doi.org/10.1016/j.watres.2014.04.035